Received 12 May 2021; revised 11 June 2021; accepted 13 June 2021. Date of publication 21 June 2021; date of current version 6 July 2021.

Digital Object Identifier 10.1109/OJAP.2021.3090927

Co-Designed 3+3 Port Dual-Band Broadside Tri-Modal Patch Antenna

CHI-YUK CHIU [1] (Senior Member, IEEE), BUON KIONG LAU [2] (Senior Member, IEEE), AND ROSS MURCH [1,3] (Fellow, IEEE)

[1]Department of Electronic and Computer Engineering, The Hong Kong University of Science and Technology, Hong Kong

[2]Department of Electrical and Information Technology, Lund University, 221 00 Lund, Sweden

[3]Institute for Advanced Study, The Hong Kong University of Science and Technology, Hong Kong

CORRESPONDING AUTHOR: C.-Y. CHIU (e-mail: eefrankie@ust.hk)

This work was supported by the Hong Kong Research Grants Council under Grant GRF 16208117.

ABSTRACT A co-designed (3+3)-port antenna for dual-band operation that requires no feeding or decoupling network is proposed and verified. The antenna consists of six ports which are divided into two groups that resonate in two different frequency ranges. The basic radiating element is a tri-modal patch in a folded snowflake-shaped structure with the largest antenna dimension of $0.48\lambda_1$ or $0.68\lambda_2$, where λ_1 and λ_2 are the wavelengths in air at the center frequencies of the lower and upper operating bands, respectively. Measurement results show that the 10 dB impedance bandwidths of the two respective bands are 19.7% and 14.4%. The proposed antenna exhibits compact, multiport, multiband and broadside radiation characteristics which are not only suitable for dual-band MIMO applications, but also for energy harvesting systems with spatial and frequency diversities, or dual-function wireless systems with simultaneous information and power transfer.

INDEX TERMS Broadside radiation, characteristic modes, multiport, multiband, multiple-input multiple-output (MIMO) antenna, shared aperture.

I. INTRODUCTION

IN RECENT wireless communications research there is a growing trend to reuse a common radiating area for providing multiple antenna ports with different operating frequency bands. This is different from a conventional multiband antenna which typically only consists of a single port. The multiport approach to realize multiband antennas is not only space saving, but it is needed when different ports are dedicated for different services. One recent example of such an antenna is a two-port circularly polarized dual-band shared-aperture ultra high frequency (UHF)/ultra-wideband (UWB) radio-frequency identification (RFID) reader antenna [1]. Its multifunctionality is achieved by placing four UHF sequential rotationally excited rectangular patches outside a UWB radiator [1]. The integration of a millimeter-wave (mm-wave) band antenna arrays into a sub-6 GHz antenna is another example of this approach of aperture area saving [2]–[4].

On the other hand, multiports can be used to provide orthogonal spatial subchannels for multiple-input, multiple-output (MIMO) operation in the same frequency band [5]–[8]. These subchannels provide a linear increase in capacity with the number of antenna ports, without requiring additional transmit power or spectral resource.

Furthermore, the number of available antenna ports can be regarded as another dimension in ambient radio frequency (RF) energy harvesting (EH) systems to collect more RF power simultaneously [9]–[13]. In RF EH, each antenna port is connected to an individual rectifier to convert RF energy into direct current (DC). Then, DC combining can be performed at the outputs of all rectifiers to raise the total output DC voltage and DC power. One major benefit of utilizing multiport antennas for EH is that space (MIMO) and frequency (multiband) diversities can be obtained in a multipath environment. Moreover, since the rectifier circuit can only achieve high energy conversion efficiency for

TABLE 1. Comparison of tri-modal snowflake-shaped patch antennas.

Tri-modal antennas	[25]/[26]	[24]	This work
No. of ports	3	3	3 + 3
No. of operating bands	1	1	2
Electrical size (λ_c) or (λ_{c1}) or (λ_{c2})*	$0.36\lambda_c \times 0.36\lambda_c \times 0.09\lambda_c$ (Patch in the air)	$0.48\lambda_c \times 0.48\lambda_c \times 0.11\lambda_c$ (Patch in the air)	$0.48\lambda_{c1} \times 0.48\lambda_{c1} \times 0.12\lambda_{c1}$ $0.68\lambda_{c2} \times 0.68\lambda_{c2} \times 0.17\lambda_{c2}$ (Patch in the air)
Reported bandwidth	4.3%	19.7%	19.7% 14.4%
Measured minimum isolation (dB)	17.0	14.3	13.7 15.2
Minimum ECC	below 0.1	0.02	0.04 0.003
Measured peak gain (dBi)†	6.9 (with circular ground plane: diameter of 100 mm)	7.5 (with circular ground plane: diameter of 100 mm)	7.9 6.1 (with circular ground plane: diameter of 100 mm)
Measured peak efficiency	96%	92%	87.2% 88.3%

*λ_c is the wavelength in air at the center frequency; λ_{c1} and λ_{c2} refer to low-band and high-band center frequencies.
† Measured peak gain is the product of measured total efficiency and directivity.

a limited bandwidth in each port, the multiport approach is favorable for increasing EH efficiency [11], [12]. In addition to ambient RF EH, the system can be used for information transfer (IT) and even localization, if a modulator/demodulator (modem) is embedded. In [14], a compact spiral antenna was used to carry out communication and localization through UWB technology and EH in the UHF band at the same time. As opposed to EH that opportunistically extracts ambient RF energy, the concept of wireless power transfer (WPT) involves a dedicated transmitter, which can be used for charging devices [15]–[18]. More advanced systems can perform simultaneous wireless information and power transfer (SWIPT) [19]–[23], but there exists a trade-off between the information and energy transmission.

In the context of creating multiports for both multiband and MIMO operations, the wideband broadside tri-modal patch antenna in [24] has undergone a further evolution, such that a single compact radiating element can be shared by two tri-port antennas working in two different frequency bands. In particular, three new ports are created to excite a new frequency band, on top of the existing tri-port setup in [24] that excites a wideband dual-resonance. A comparison of the features and performance of the proposed antenna and existing tri-modal snowflake-shape patch antenna variants is provided in Table 1. It is noted that comparisons of a previous (single-band) variant of the proposed antenna with two other (single-band) tri-port patch antennas have been provided in [24, Table 1]. Like its predecessors [24]–[26], the (3+3)-port design uses only capacitive feeds and requires

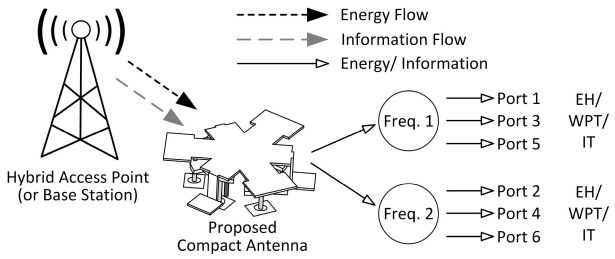

FIGURE 1. Receiver schematic with dual-band energy and data transmission enabled.

no feeding or decoupling network. In addition, all six ports are available for use all the time, hence no switching is needed. Figure 1 illustrates the flexible usage of the proposed compact six-port antenna that supports dual-band operation. The number of ports used for energy or information-related transmission can be adjusted subject to the needs and receiver circuitry. For example, three ports can be used for WPT at Frequency 1, whereas the remaining three ports can be allocated for IT at Frequency 2. When there is no dedicated power source nor IT, then all six ports can be used for EH. Moreover, since the three new ports also provide broadside patterns, the dual-band antenna can also be used as array elements for dual-band massive MIMO application.

This paper is organized as follows. In Section II, the systematic design procedure underlying the proposed dual-band antenna is provided. The evolution from a broadside tri-modal patch antenna element is described using characteristic mode analysis (CMA). Then, Section III provides the

detailed geometry and dimensions of the proposed antenna. Two groups of antenna ports corresponding to two different resonant frequencies are circularly interlaced to provide dual-band operation. In Section IV, the radiation performance of the two groups of antenna ports is reported. Both simulation and measurement results of *S*-parameters, antenna gains, total efficiencies and radiation patterns are included. Then, a set of four dual-band tri-modal patch elements with half-wavelength center-to-center element spacings is used to explore the array performance in Section V. Finally, conclusions are drawn in Section VI.

II. SYSTEMATIC DESIGN PROCEDURE

This section consists of two parts. The recently developed wideband snowflake-shaped patch antenna [24] is first revisited. By analyzing the characteristic modes (CMs) at the high frequency band, potential regions for accommodating additional antenna ports are identified. Then, the details on how the tri-port antenna is evolved to become a (3+3)-port antenna for dual-band operation are provided.

REVISITING WIDEBAND SNOWFLAKE-SHAPED PATCH ANTENNA

The proposed co-designed (3+3)-port antenna is based on the structure of the broadside tri-modal patch [24], which consists of a folded snowflake-shaped radiator excited by three capacitive loading plates underneath, as depicted in Figs. 2(a) and 2(b). It is noted that both the snowflake-shaped radiator and the loading capacitive plates possess third order rotational symmetry when viewed from the top, which enables identical impedance matching and radiation performance from all three antenna ports. The tri-port antenna exhibits wideband radiation property because two sets of three CMs, i.e., modes 1, 2, 3 and modes 4, 5, 6 in Fig. 2(c), have been utilized to produce dual resonances at each port. At each resonance, three CMs are excited simultaneously, including two broadside patterns and one non-broadside pattern, enabling three antenna ports with broadside radiation to be achieved with low pattern correlation. The eigenvalues in Fig. 2(c) were obtained using the CMA feature of Altair FEKO [27]. In this work, it is observed that modes 4, 5 and 6 retain moderate eigenvalues from 3.6 GHz onwards (the highlighted region in the figure), which means that the snowflake-shaped radiator has the potential to be slightly modified to support an even wider bandwidth operation or additional antenna ports at the higher frequency range. When the capacitive loading plates in Fig. 2(b) are revisited, it can be seen that the regions highlighted in red can be used to accommodate three more antenna ports without increasing the overall antenna size or sacrificing the rotational symmetry. With this in mind, the possibility of achieving (3+3)-port dual-band broadside antenna is investigated using CMA.

To study modes 4-6 more closely, the modal significance (MS) of the structure is plotted up to 6 GHz in Fig. 3. It should be noted that the twelve modes illustrated in the figure are numbered by their MS values at 2 GHz (i.e., mode 1

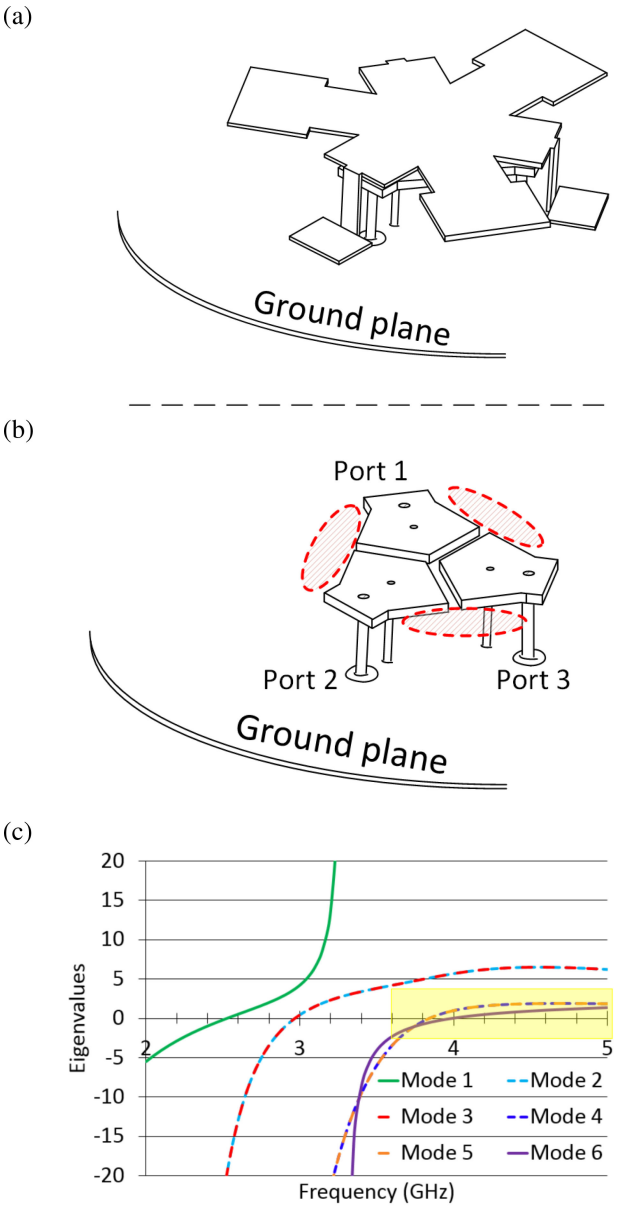

FIGURE 2. Broadside tri-modal patch antenna in [24]: (a) overall structure; (b) capacitive loading plates with shorting pins; (c) eigenvalues (first six modes).

has the largest MS value, etc.). Modes 4-6 in Fig. 2(c) correspond to modes 11, 12 and 9, respectively. It is noted that the MS of these modes is above 0.5 at 5.5 GHz. Therefore, the amplitude and phase of the characteristic electric field (E-field) distributions under the radiator are examined at 5.5 GHz (see Fig. 4). It is observed that high E-fields are present inside the black, red and white boxes over the three modes (see Figs. 4(a)–4(c)). In addition, the phase distributions within these boxes (see Figs. 4(d)–4(f)) follow similar behavior as in [24] and [26]. For example, if two individual ports are located in the black and white boxes, respectively, then a 180° phase difference is obtained between the excitation of the second mode by the two ports. This would introduce a negative term in the complex correlation of the

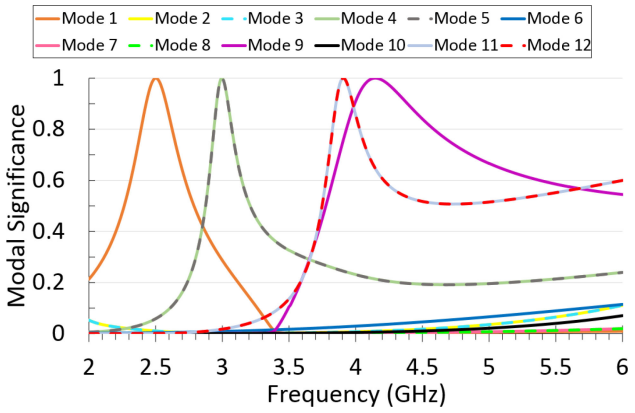

FIGURE 3. Modal significance of broadside tri-modal patch antenna in [24].

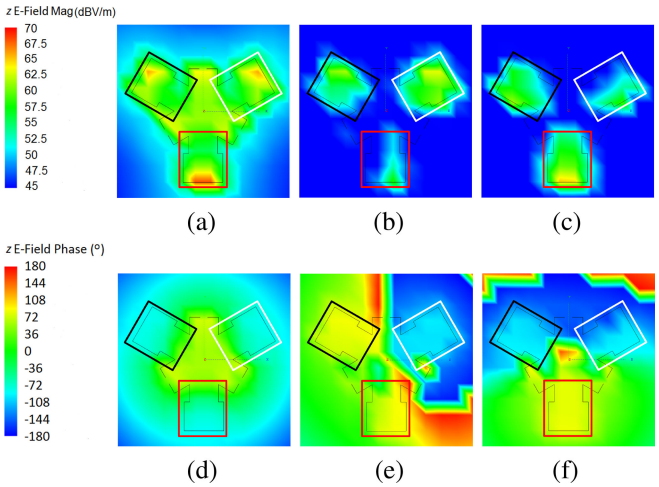

FIGURE 4. The *z*-directed characteristic E-fields at 0.2 mm below the top snowflake patch in [24]: amplitude distribution of the first three modes at 5.5 GHz correspond to (a)–(c); phase distribution of the first three modes at 5.5 GHz correspond to (d)–(f).

two port's far-field patterns, i.e., (11) in [26], which helps to lower their complex correlation. The same phenomenon can be observed from the black and red boxes of the third mode (see Fig. 4(f)). Therefore, three probes can be added to the regions below the radiator that are bounded by the black, red and white boxes, to produce a high-band resonance at 5.5 GHz, while achieving pattern orthogonality between these new ports. More importantly, the third order rotational symmetry can still be preserved after this modification.

EVOLUTION OF CAPACITIVE PLATES FOR HIGH-BAND EXCITATION

Guided by the above analysis, the three original loading plates should be split into six, to allow these new probes to be connected to separate loading plates than the three original ports used to excite the low band. The six loading plates can all be arranged at the same height and subjected to the same air gap size, or divided into two groups subjected to different air gap sizes, from the above snowflake-shaped radiator. In this work, the new three loading plates are lowered such that they can be used to facilitate higher frequency

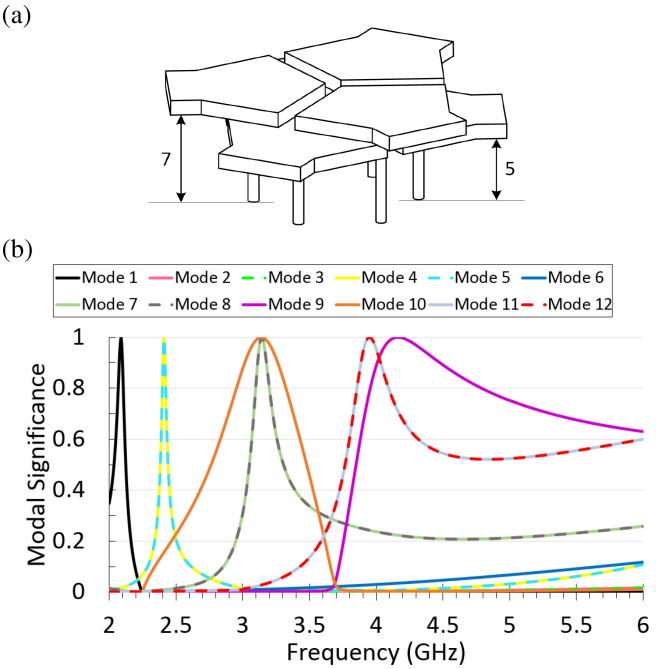

FIGURE 5. Broadside tri-modal patch antenna in [24] with newly added capacitive loading plates: (a) geometry of six capacitive loading plates (units: mm); (b) modal significance.

resonances (e.g., 5.5 GHz). However, it is also necessary to check whether the additional splitting of the loading plates will deteriorate the low frequency band resonances.

Figure 5 shows the geometry and MS of the snowflake-shaped radiator [24] with six capacitive loading plates underneath at two different heights above the ground plane (5 mm and 7 mm), but without the feeding probes. The newly added lower plates are displaced in angle by 60° with respect to the original upper plates. The first twelve modes are plotted in the figure, and as before they are numbered by their MS values at 2 GHz. Compared to Fig. 3, it is observed that the two original sets of three modes excited by 3 ports for dual resonances [24] still exist, but the frequencies of the lower resonances (modes 7, 8 and 10) have increased from 2.4 GHz to 3.15 GHz. In addition, a new set of three CMs (modes 1, 3 and 4) become resonant between 2 GHz to 2.5 GHz due to the splitting of the three loading plates into six. The modal patterns of the three CMs at 2.1 GHz and 2.4 GHz are monopole and broadside, respectively. Since their near-fields are similar to the two original sets of modes in [24], they can be excited by the existing three ports to provide an additional resonance. Furthermore, Fig. 5(b) shows that the MS of the third set of three CMs (modes 9, 11 and 12, resonant at around 4 GHz) retains high values (>0.5) up to 6 GHz. Following the analysis of the modal properties at 5.5 GHz in Section II-A, it can be expected that another three probes connected to the newly added capacitive loading plates can excite the snowflake-shaped radiator in the higher frequency range.

The first advantage of using capacitive loading plates to excite the radiator is that it provides flexibility in frequency

tuning. As can be seen, the MSs of the three dominant CMs in the proposed structure for the high band resonance maintain high values from 4.5 GHz to 6 GHz. This implies the antenna has the potential to be excited in that frequency range. The capacitance introduced between the radiator and the loading plate can be used to tune the resonant frequency of the antenna [28], i.e., a larger plate or a smaller gap between radiator and plate decreases the resonant frequency. Therefore, the size of the loading plate and its height above the ground plane are two critical parameters for the high-band excitation. The second advantage of using capacitive loading plates to excite the radiator is that the influence among the ports can be minimized, i.e., the low-band and high-band excitations can be adjusted individually by using separate plates. Furthermore, the shorting pin added to each loading plate helps to enhance the impedance matching. This is particularly important for feeding probes that are subjected to certain location constraints.

For the final structure, the overlaps between the 6 loading plates are removed. The corresponding MSs of the final structure are plotted in Fig. 6. In this case, the probe feeds are included as shorts in the FEKO simulation, as typically performed for CMA on structures with feeds. It can be seen that the antenna has the potential to excite the first two sets of CMs to produce dual resonances around 3.5 GHz to 4.5 GHz using its original three ports, as in [24]. Moreover, it also can utilize its three new ports to excite the third set of CMs to produce resonances at around 5.5 GHz. Compared with Fig. 5, it is observed that the size reduction of capacitive loading plates and the insertion of probe feeds not only alter the bandwidths of the modes, but also move resonances to the higher frequency range. This shift has in fact enhanced the MS of the dominant modes at the high band, while allowing the low-band dual resonance to be maintained. The high MS at the high band also facilitates better impedance bandwidth than the original intention of exciting these modes with MS of between 0.5-0.6.

A summary of the proposed antenna working mechanism is:

- The original tri-port snowflake-shaped patch antenna exhibits wideband radiation property utilizing two sets of three CMs.
- By further analysis, one set of three CMs retain moderate eigenvalues at the higher frequency range, which means that the snowflake-shaped radiator has the potential to support additional ports at that frequency range.
- Locations of additional ports are identified due to the observed 180° phase difference in the modal electric nearfields, which introduces a negative term in the complex correlation of any two ports' far-field patterns (resulting in low correlation among the additional ports).
- To facilitate the high-band resonance, the excitation should be less capacitive, resulting in lower capacitive loading plates being required.

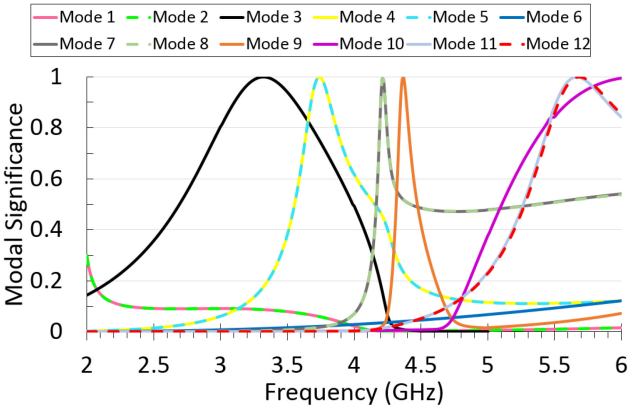

FIGURE 6. Modal significance of proposed antenna structure with all six probes replaced by shorts.

- Two groups (3+3) of antenna ports corresponding to two different resonant frequencies are circularly interlaced to provide dual-band operation.

III. CO-DESIGNED DUAL-BAND BROADSIDE TRI-MODAL PATCH ANTENNAS

In the previous section, the original design in [24] has been evolved by introducing three additional capacitive loading plates with shorting pins to the structure in the red regions indicated in Fig. 2(b), leading to a (3+3)-port dual-band antenna.

Figure 7 shows the geometry of the modified six-port broadside tri-modal patch antenna. From Fig. 7(a), it is observed that the snowflake-shaped radiator can be decomposed into two Y-shaped structures with different sizes (pink and green dashed lines encircled). It has been shown that the different sizes and loading conditions (with or without folded parts) help to create the dual resonances that were used to widen the impedance bandwidth of the antenna [24]. Furthermore, the three newly added capacitive loading plates are lower in height to help excite the resonance at the high frequency band. The larger spacing between the radiator and each of these new plates provides a smaller capacitance, resulting in a less-capacitive feed to excite the antenna in the higher frequency band. The geometry of the loading plates are simplified into radial shapes to ease prototyping and to avoid any overlap. The largest dimension given in the figure is 37.1 mm and the material used is 0.5 mm-thick copper (for ease of folding). The pink and green capacitive loading plates are of different heights, which help to set the resonant frequency of the respective antenna ports. In particular, the pink plates that are fed by ports 1, 3 and 5 excite three modes of the patch at each of the two resonances, as in [24], resulting in a wideband performance. On the other hand, the green plates that are fed by ports 2, 4 and 6 are introduced in this work to excite three other modes at a higher band.

In Fig. 7(b), it can be seen that there are six capacitive loading plates distributed in a circular arrangement under the snowflake-shaped radiator. Each loading plate is connected

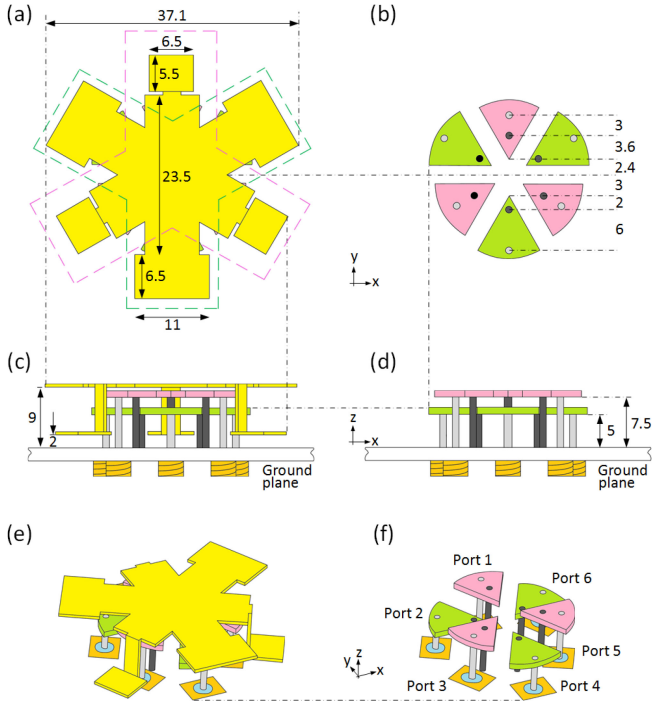

FIGURE 7. Geometry of proposed co-designed two broadside tri-modal patch antennas (units: mm): (a) plan view; (b) plan view without radiator; (c) side view; (d) side view without radiator; (e) perspective view; and (f) perspective view without radiator.

to one coaxial probe (grey circle) and one 1 mm-diameter copper shorting pin (black circle). Although the feed and shorting pin on each plate can be placed at arbitrary locations along the plate for impedance matching, they are aligned along the center line of the plate to enhance the radiation pattern symmetry. In addition to impedance matching, it is found that by sliding the feed position along the line, the resonant frequency at the port will also be changed. For example, when the feeds for ports 2, 4 and 6 are moved towards their respective shorting pins, the resonant frequency at the high-band decreases.

The six plates are made of 1 mm-thick copper and can be regarded as one sixth of a circle, but the radii of plates in pink and green are 8.8 mm and 9.2 mm, respectively. It is noted that the radii of plates also provide some flexibility in fine tuning the resonant frequencies. For example, the resonant frequency at the high-band will shift up by about 2% if all six plates have the radii of 8.8 mm. The side views of the proposed antenna with and without the radiator are depicted in Figs. 7(c) and 7(d), in which SubMiniature version A (SMA) connectors can be seen at the bottom. The ground is printed on both sides of a circular FR-4 epoxy board with a diameter of 100 mm. It should be noted that the radiator does not touch to the capacitive loading plates nor ground plate. Foam material is used to support the radiator in the prototype. Figures 7(e) and 7(f) show the three-dimensional geometry with and without the snowflake-shaped radiator. The six ports arrangement is also provided in which ports 1 and 4 are lying on the *yz*-plane. It can be seen that the co-designed dual-band broadside tri-modal patch antennas retains the third order rotational symmetry of its predecessors [24]–[26], where ports 1, 3 and 5, and ports 2, 4 and 6 are two sets of three ports that share similar matching and radiation performances.

One challenge of prototyping the antenna is in accommodating six SMA connectors within a small area. Therefore, the locations of antenna probes cannot be too close to the center and this reduces the flexibility to improve matching and adjust resonant frequency by changing probe locations. On the other hand, the locations of shorting pins and the separations between adjacent capacitive loading plates can also be utilized to adjust the impedance matching.

To further verify that the three resonances generated by the proposed antennas are mainly contributed from the three sets of CMs shown in Fig. 6, the complex correlation coefficients (CCCs) of the port pattern with each modal pattern (of interest) are computed at 3.65 GHz, 4.30 GHz and 5.80 GHz, based on the results in Fig. 6. The computed CCCs are provided in Table 2. It is noted that ports 1 and 4 are the excited antenna ports for calculating CCCs at the first two and third resonances, respectively. The other five unexcited ports are terminated with 50 ohm loads. The first six modes at each resonance are calculated and the modes are numbered by their MS values at their respective three frequencies. We also map these modes to Fig. 6, which show that the three sets of CMs (modes 3, 4, 5; modes 7, 8, 9; modes 10, 11, 12) are indeed excited. Due to the narrowband characteristic of modes 7-9, the contributions of the second resonance are not as clearly attributed to these three modes as those of the other two resonances. Modes 4 and 5 are found to also provide 16% and 9% in the radiated power of port 1, respectively. Nevertheless, modes 7, 8 and 9 do contribute substantially in power (65%) at 4.30 GHz.

In summary, the five antenna design steps are:

1) Use the wideband snowflake-shaped patch antenna as a starting point.
2) Analyze the MS of the antenna structure at the high band.
3) Determine the locations of additional ports from the characteristic E-fields at the high band and add additional capacitive plates.
4) Adjust the additional capacitive plates' size and height for high-band excitation.
5) Fine tune the dimensions of the antenna structure to facilitate both low-band and high-band resonances.

IV. ANTENNA PERFORMANCE

In this section, both simulation and measurement results of *S*-parameters, antenna gains, total efficiencies and radiation patterns are presented for validating the proposed antenna design. The simulation is performed in the time-domain solver of the 2020 CST Microwave Studio Suite [29]. The dimensions of the prototype shown in Fig. 8 are the same as those provided in Fig. 7.

TABLE 2. Computed complex correlation coefficients.

Frequency	1st mode	2nd mode	3rd mode	4th mode	5th mode	6th mode
3.65 GHz (Port 1)	0.589 ∠ 159.74° Mode 3*	0.490 ∠ -157.33° Mode 4*	0.624 ∠ 22.71° Mode 5*	0.162 ∠ -97.00° Mode 1*	0.109 ∠ -96.39° Mode 2*	0.004∠ 114.69° Mode 6*
4.30 GHz (Port 1)	0.213 ∠ 160.40° Mode 7*	0.155 ∠ 159.86° Mode 8*	0.765 ∠ 32.29° Mode 9*	0.397 ∠ 124.70° Mode 4*	0.308 ∠ 125.18° Mode 5*	0.001 ∠ -14.08° Mode 6*
5.80 GHz (Port 4)	0.716 ∠ 163.48° Mode 11*	0.304 ∠ 162.93° Mode 12*	0.576 ∠ 10.92° Mode 10*	0.192 ∠ 122.66° Mode 7*	0.072 ∠ 120.45° Mode 8*	0.118 ∠ -80.69° Mode 4*

*Corresponding mode number mapped to Fig. 6.

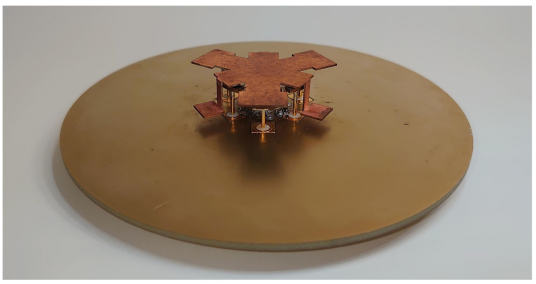

FIGURE 8. Prototype of co-designed two broadside tri-modal patch antenna.

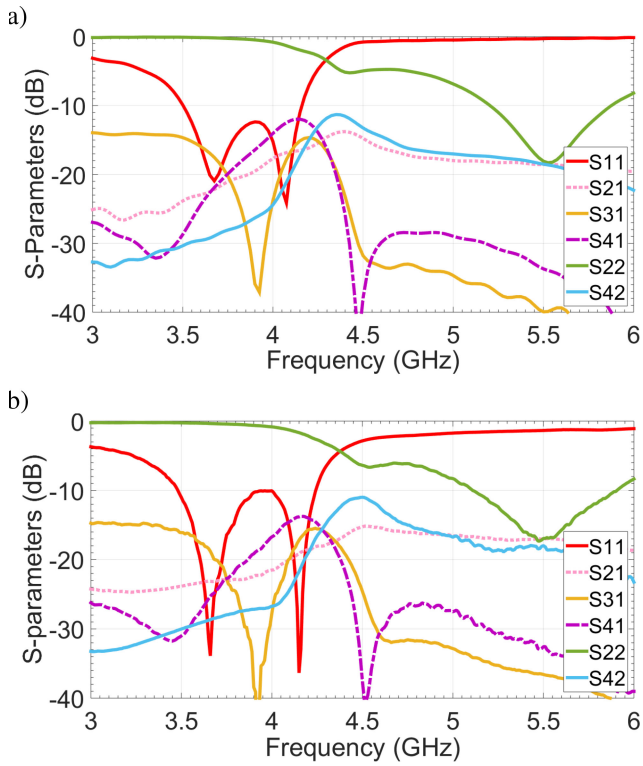

FIGURE 9. *S*-parameters of co-designed two broadside tri-modal patch antennas: (a) simulation; (b) measurement.

Figure 9 shows *S*-parameters of the proposed dual-band tri-modal patch antennas. It should be noted that due to the third order rotational symmetry of the structure, ports

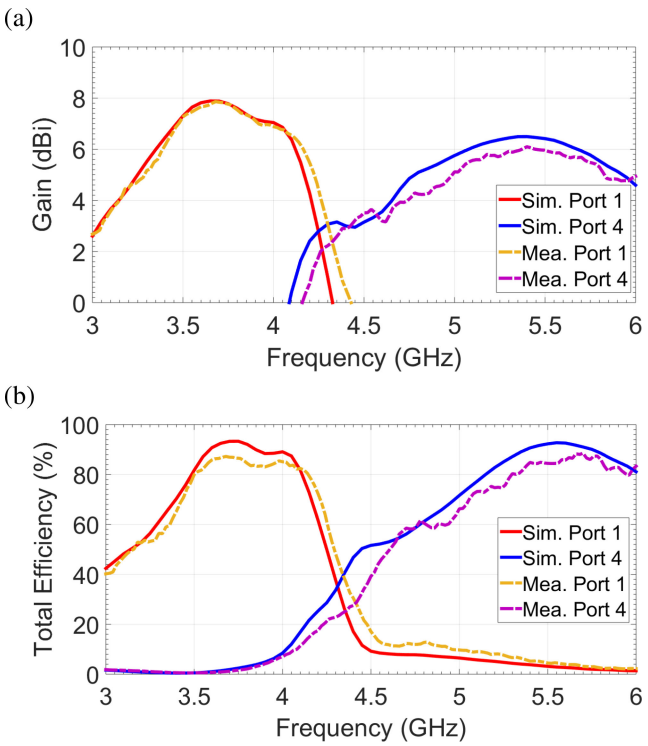

FIGURE 10. Radiation performance of co-designed two broadside tri-modal patch antennas: (a) gains of ports 1 and 4; (b) efficiencies of ports 1 and 4.

3 and 5, and ports 4 and 6 will exhibit the same radiation performance as port 1 and port 2, respectively (subjected to 60° or 120° rotation along ϕ). Similarly, several mutual coupling combinations will be the same, such as $S_{21} = S_{32}$. It can be seen that port 1 offers a simulated 10 dB impedance bandwidth from 3.50 GHz to 4.15 GHz, which agrees well with the measured bandwidth from 3.48 GHz to 4.25 GHz. For port 2, the simulated 10 dB impedance bandwidth is from 5.20 GHz to 5.88 GHz, which is also close to the measured result of 5.11 GHz to 5.90 GHz. In terms of measured fractional bandwidth and largest antenna dimension at the center frequency, port 1 offers 19.7% bandwidth for the size of $0.48\lambda_1$, whereas port 2 yields 14.4% bandwidth for the size of $0.68\lambda_2$, where λ_1 and λ_2 are the free space

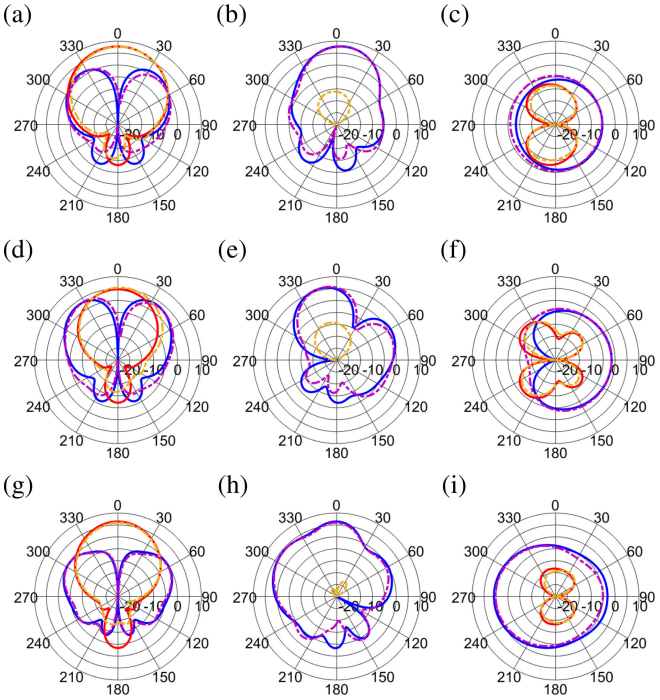

FIGURE 11. Radiation patterns of co-designed two broadside tri-modal patch antennas with simulation (solid), measurement (dash-dot), *E*-phi (red/ orange), and *E*-theta (blue/ violet). Port 1 at 3.7 GHz is (a)-(c), port 1 at 4.1 GHz is (d)-(f), and port 4 at 5.5 GHz is (g)-(i). The *xz*-plane is in (a), (d) and (g); the *yz*-plane is in (b), (e) and (h); and the *xy*-plane is in (c), (f) and (i).

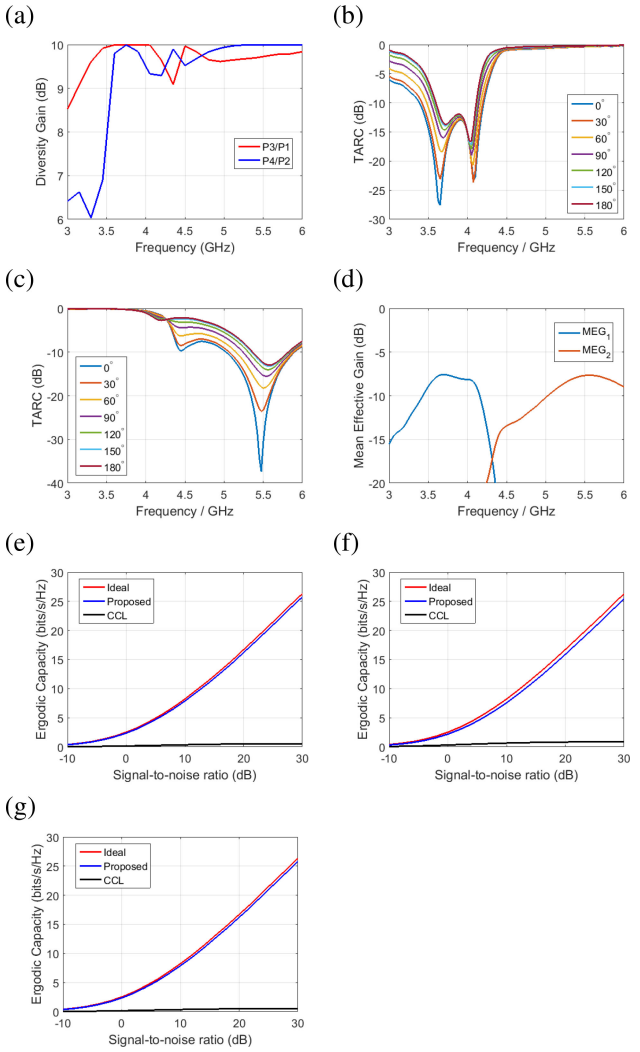

FIGURE 12. MIMO performance of co-designed two broadside tri-modal patch antennas: (a) diversity gain; (b) TARC of port 1 (c) TARC of port 2; (d) MEG; (e) ergodic capacity at 3.7 GHz; (f) ergodic capacity at 4.1 GHz; (g) ergodic capacity at 5.5 GHz.

wavelengths at the center frequencies of the two bands (i.e., 3.865 and 5.505 GHz). In addition, most of the coupling coefficients are below −15 dB in the two frequency bands. The minimum isolation S_{41} is found at around 4.1 GHz to 4.2 GHz. This is due to the E-fields at these frequencies are also high at the high-band feed positions, causing increased coupling across the two frequency bands. Owing to the orientation of the antenna ports, port 2 does not align with the *xz*-plane nor the *yz*-plane. To better reflect the far-field results particularly for radiation patterns, port 4 is chosen instead of port 2 to represent the performance of the second group of antennas. Figure 10 shows simulated and measured gains and total efficiencies of the proposed antenna. It is found that the peak gains and total efficiencies measured from port 1 and port 4 are 7.86 dBi and 87.2%, and 6.10 dBi and 88.3%, respectively. The radiation patterns in three standard cuts taken from port 1 and port 4 are presented in Fig. 11. The results show that the measurements and simulations agree well with each other. Broadside radiation patterns are obtained over the two frequency bands from the two antenna ports.

In Fig. 12, several MIMO metrics are also provided based on simulation results, which include diversity gain, total active reflection coefficient (TARC), mean effective gain (MEG), and ergodic capacity. The 3 × 3 ergodic capacity results were obtained for the case of no channel knowledge at the transmitter, as well as 100% total efficiency and no correlation of the transmit antennas. The results for both ideal and the proposed antennas at the receiving side were calculated. It should be noted that due to the rotation symmetry of ports 1, 3, 5 and ports 2, 4, 6, some ports results are duplicated and so omitted in the figures for simplicity. For Figs. 12(e)–(g), the channel capacity losses (CCL) at 3.7 GHz, 4.1 GHz and 5.5 GHz can also be obtained by taking the difference of ergodic 3 × 3 capacity between the ideal case of complex independent and identically distributed (iid) channels (with no efficiency loss or correlation due to the antennas) and the case with correlation and efficiencies included [30].

V. MIMO ARRAY DISCUSSIONS

With the third order rotational symmetry, the proposed co-designed two broadside tri-modal patch antenna is inherently suitable for concatenating as a MIMO array, e.g., for massive MIMO operation [24]. The rotational symmetry provides a balanced environment for identical matching and radiation

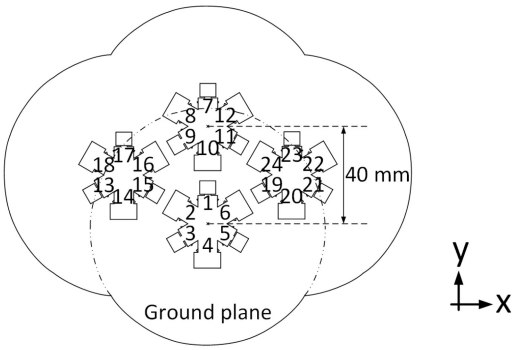

FIGURE 13. Geometry of four elements co-designed two broadside tri-modal patch MIMO array.

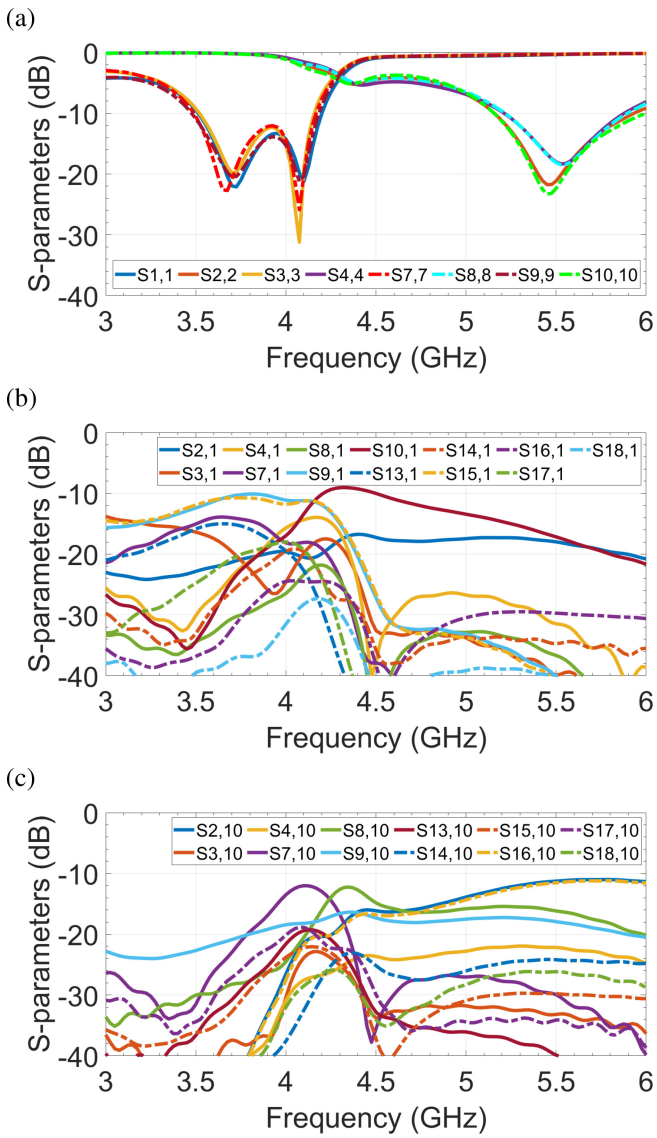

FIGURE 14. Simulated *S*-parameters of co-designed two broadside tri-modal patch MIMO array: (a) reflections; (b) mutual couplings w.r.t. port 1; (c) mutual couplings w.r.t. port 10.

performances when elements are arranged in 60° translation as illustrated in Fig. 13. For simplicity, the array only consists of four elements (24 ports), but it is sufficient to

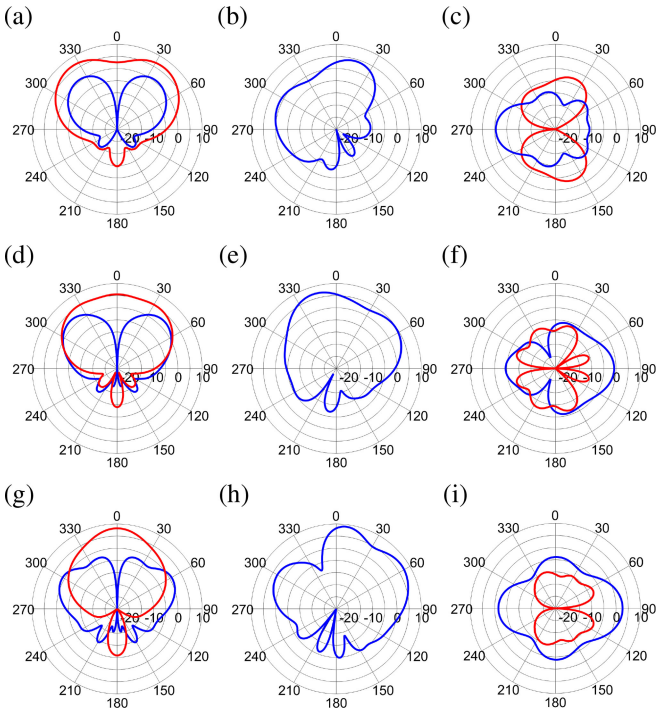

FIGURE 15. Simulated radiation patterns of co-designed two broadside tri-modal patch MIMO array with *E*-phi (red), and *E*-theta (blue). Port 1 at 3.7 GHz is (a)-(c), port 1 at 4.1 GHz is (d)-(f), and port 10 at 5.5 GHz is (g)-(i). The *xz*-plane is in (a), (d) and (g); the *yz*-plane is in (b), (e) and (h); and the *xy*-plane is in (c), (f) and (i).

capture the main (first-order) effects of neighboring elements. In the figure, the center-to-center spacings are kept in 40 mm for all elements, which is equivalent to $0.52\lambda_1$ and $0.73\lambda_2$, respectively. It should be noted that the numbers shown in the figure refer to the antenna port numbers: Ports with odd and even numbers correspond to the low-band and high-band excitations, respectively. The dimensions of the snowflake-shaped radiators and capacitive loading plates are as given in Fig. 7. The array ground plane is merged from the circular ground plane of each element (diameter of 100 mm).

Figure 14(a) shows the reflection coefficients of eight representative ports. In the array design, although no specific mutual coupling suppression technique has been adopted, the coupling effects among all broadside tri-modal patch elements have not severely deteriorated the low-band and high-band resonances. The two 10 dB impedance bandwidths of different ports are generally preserved when compared to those of the single element given in Fig. 9(a).

The mutual coupling coefficients with respect to ports 1 and 10 are provided in Figs. 14(b) and 14(c), respectively. The two ports are selected as they are located in the middle and fully surrounded by other ports. Therefore, ports 1 and 10 can be used for quantifying mutual couplings corresponding to the ports with low-band and high-band excitations in general. Due to the geometrical symmetry, some port combinations can be omitted in the figures. It is found that all couplings are lower than −10 dB, and

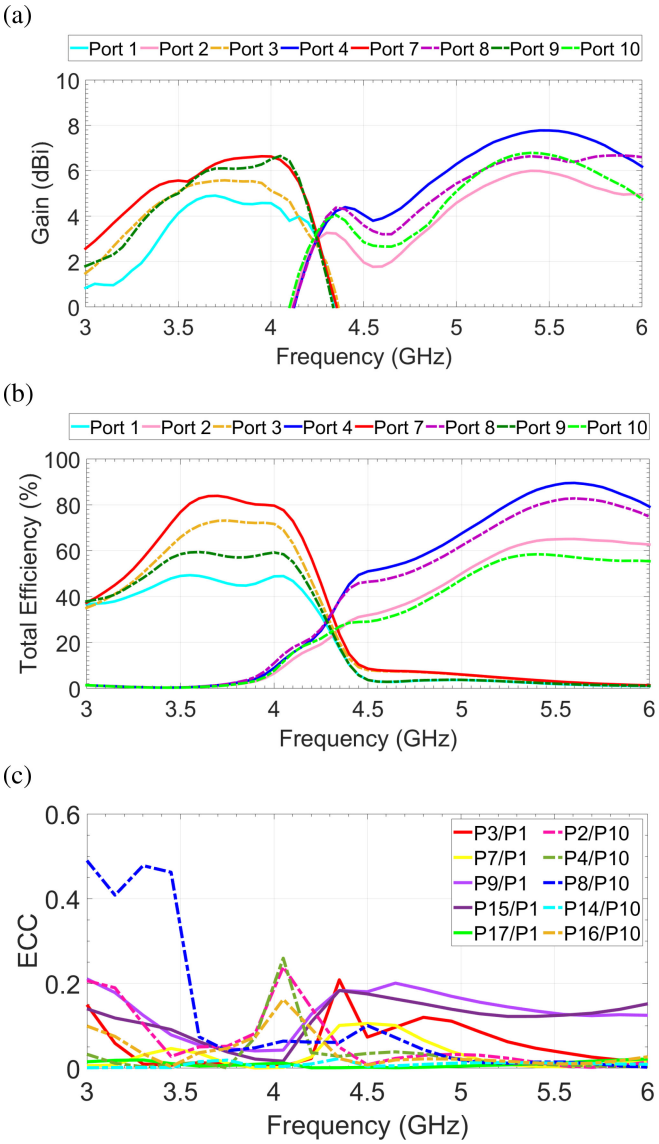

FIGURE 16. Simulated radiation performance of co-designed two broadside tri-modal patch MIMO array: (a) gain; (b) efficiency; (c) envelope correlation coefficient.

most of them are below −14 dB and −22 dB for low-band and high-band resonances, respectively. In the proposed array configuration, the two dominant factors contributing to mutual coupling level are the relative separation and in-band operation of the two elements. To further reduce mutual coupling effects, shorting/choke walls can be utilized in between every two adjacent elements. However, this involves a trade-off between coupling performance and more complicated fabrication process.

In addition to the *S*-parameters, the radiation performances are also examined for the array of four co-designed two broadside tri-modal patch elements. The radiation patterns of the proposed antenna array of port 1 at 3.7 GHz and 4.1 GHz and port 10 at 5.5 GHz are provided in Fig. 15. Figures 16(a) and 16(b) show the gains and efficiencies of eight representative antenna ports. The envelope correlation coefficients (ECCs) calculated from different port far-field radiation patterns are depicted in Fig. 16(c). The ECCs of the proposed dual-band array elements should be analyzed in two separate frequency bands (low-band and high-band) according to the port combinations with odd or even numbers, i.e., dash lines and solid lines correspond to low-band and high-band ECCs, respectively.

VI. CONCLUSION

In this paper, a co-designed (3+3)-port antenna for dual-band operation is proposed and tested. The fundamental working principle of the antenna is similar to the existing wideband broadside tri-modal patch antenna. By introducing three additional capacitive loading plates and adjusting their heights, a single radiator can be shared by two groups of tri-modal patch antennas working at different frequency bands. The proposed antenna is not only intended for use as massive MIMO element (unit cell) as in previous snowflake-shaped patch designs, but also opens up a new possibility of fully utilizing the antenna aperture for energy and information transmission.

REFERENCES

[1] J. Zhang and Z. Shen, "Dual-band shared-aperture UHF/UWB RFID reader antenna of circular polarization," *IEEE Trans. Antennas Propag.*, vol. 66, no. 8, pp. 3886–3893, Aug. 2018.

[2] J. Kurvinen, H. Kähkönen, A. Lehtovuori, J. Ala-Laurinaho, and V. Viikari, "Co-designed mm-Wave and LTE handset antennas," *IEEE Trans. Antennas Propag.*, vol. 67, no. 3, pp. 1545–1553, Mar. 2019.

[3] M. Ikram, E. A. Abbas, N. Nguyen-Trong, K. H. Sayidmarie, and A. Abbosh, "Integrated frequency-reconfigurable slot antenna and connected slot antenna array for 4G and 5G mobile handsets," *IEEE Trans. Antennas Propag.*, vol. 67, no. 12, pp. 7225–7233, Dec. 2019.

[4] J. Lan, Z. Yu, J. Zhou, and W. Hong, "An aperture-sharing array for 3.5/28 GHz terminals with steerable beam in millimeter wave band," *IEEE Trans. Antennas Propag.*, vol. 68, no. 5, pp. 4114–4119, May 2020.

[5] S. K. Chaudhury, W. L. Schroeder, and H. Chaloupka, "MIMO antenna system based on orthogonality of the characteristic modes of a mobile device," in *Proc. 2nd Int. ITG Conf. Antennas*, Munich, Germany, Mar. 2007, pp. 58–62.

[6] H. Li, Z. T. Miers, and B. K. Lau, "Design of orthogonal MIMO handset antennas based on characteristic mode manipulation at frequency bands below 1 GHz," *IEEE Trans. Antennas Propag.*, vol. 62, no. 5, pp. 2756–2766, May 2014.

[7] M. Y. Li *et al.*, "Eight-port orthogonally dual-polarized antenna array for 5G smartphone applications," *IEEE Trans. Antennas Propag.*, vol. 64, no. 9, pp. 3820–3830, Sep. 2016.

[8] L. Sun, Y. Li, Z. Zhang, and Z. Feng, "Wideband 5G MIMO antenna with integrated orthogonal-mode dual-antenna pairs for metal-rimmed smartphones," *IEEE Trans. Antennas Propag.*, vol. 68, no. 4, pp. 2494–2503, Apr. 2020.

[9] N. Shinohara and H. Matsumoto, "Experimental study of large rectenna array for microwave energy transmission," *IEEE Trans. Microw. Theory Techn.*, vol. 46, no. 3, pp. 261–268, Mar. 1998.

[10] Z. Popović *et al.*, "Scalable RF energy harvesting," *IEEE Trans. Microw. Theory Techn.*, vol. 62, no. 4, pp. 1046–1056, Apr. 2014.

[11] S. Shen, C.-Y. Chiu, and R. D. Murch, "A dual-port triple-band L-probe microstrip patch rectenna for ambient RF energy harvesting," *IEEE Antennas Wireless Propag. Lett.*, vol. 16, pp. 3071–3074, 2017.

[12] S. Shen, C.-Y. Chiu, and R. D. Murch, "Multiport pixel rectenna for ambient RF energy harvesting," *IEEE Trans. Antennas Propag.*, vol. 66, no. 2, pp. 644–656, Feb. 2018.

[13] S. Shen, Y. Zhang, C.-Y. Chiu, and R. Murch, "An ambient RF energy harvesting system where the number of antenna ports is dependent on frequency," *IEEE Trans. Microw. Theory Techn.*, vol. 67, no. 9, pp. 3821–3832, Sep. 2019.

[14] M. Fantuzzi, D. Masotti, and A. Costanzo, "A novel integrated UWB–UHF one-port antenna for localization and energy harvesting," *IEEE Trans. Antennas Propag.*, vol. 63, no. 9, pp. 3839–3848, Sep. 2015.
[15] D. Arnitz and M. S. Reynolds, "Multitransmitter wireless power transfer optimization for backscatter RFID transponders," *IEEE Antennas Wireless Propag. Lett.*, vol. 12, pp. 849–852, 2013.
[16] C. R. Valenta and G. D. Durgin, "Harvesting wireless power: Survey of energy-harvester conversion efficiency in far-field, wireless power transfer systems," *IEEE Microw. Mag.*, vol. 15, no. 4, pp. 108–120, Jun. 2014.
[17] Energous. *Energous Receives Industry-First FCC Certification for Over-the-Air, Power-at-a-Distance Wireless Charging*. Accessed: Dec. 26, 2017. [Online]. Available: https://ir.energous.com/press-releases/detail/596/energous-receives-industry-first-fcc-certification-for
[18] C. Peng *et al.*, "On the load-independence of a multi-receiver wireless power transfer system," *IEEE Microw. Wireless Compon. Lett.*, vol. 29, no. 8, pp. 563–565, Aug. 2019.
[19] R. Zhang and C. K. Ho, "MIMO broadcasting for simultaneous wireless information and power transfer," *IEEE Trans. Wireless Commun.*, vol. 12, no. 5, pp. 1989–2001, May 2013.
[20] D. W. K. Ng, E. S. Lo, and R. Schober, "Robust beamforming for secure communication in systems with wireless information and power transfer," *IEEE Trans. Wireless Commun.*, vol. 13, no. 8, pp. 4599–4615, Aug. 2014.
[21] S. Bi, C.-K. Ho, and R. Zhang, "Wireless powered communication: Opportunities and challenges," *IEEE Commun. Mag.*, vol. 53, no. 4, pp. 117–125, Apr. 2015.
[22] E. Boshkovska, D. W. K. Ng, N. Zlatanov, and R. Schober, "Practical non-linear energy harvesting model and resource allocation for SWIPT systems," *IEEE Commun. Lett.*, vol. 19, no. 12, pp. 2082–2085, Dec. 2015.
[23] T. D. P. Perera, D. N. K. Jayakody, S. K. Sharma, S. Chatzinotas, and J. Li, "Simultaneous wireless information and power transfer (SWIPT): Recent advances and future challenges," *IEEE Commun. Surveys Tuts.*, vol. 20, no. 1, pp. 264–302, 1st Quart., 2018.
[24] C. Y. Chiu, B. K. Lau, and R. Murch, "Bandwidth enhancement technique for broadside tri-modal patch antenna," *IEEE Open J. Antennas Propag.*, vol. 1, pp. 524–533, 2020.
[25] C. Y. Chiu and R. Murch, "Compact integrated three-broadside-mode patch antenna," U.S. Patent Appl. 16 220 916, Dec. 14, 2018.
[26] C.-Y. Chiu, S. Shen, B. K. Lau, and R. Murch, "The design of a tri-modal broadside antenna element for compact massive MIMO arrays," *IEEE Antennas Propag. Mag.*, vol. 62, no. 6, pp. 46–61, Dec. 2020.
[27] *FEKO v2020.1.2*, Altair Eng., Inc., Troy, MI, USA, 2020.
[28] C.-Y. Chiu, K. M. Shum, and C. H. Chan, "A tunable via-patch loaded PIFA with size reduction," *IEEE Trans. Antennas Propag.*, vol. 55, no. 1, pp. 65–71, Jan. 2007.
[29] *CST Studio Suite*, Dassault Systèmes, 2020.
[30] R. Tian, B. K. Lau, and Z. Ying, "Multiplexing efficiency of MIMO antennas," *IEEE Antennas Wireless Propag. Lett.*, vol. 10, pp. 183–186, 2011.

CHI-YUK CHIU (Senior Member, IEEE) received the B.Eng., M.Eng., and Ph.D. degrees in electronic engineering from the City University of Hong Kong in 2001, 2001 and 2005, respectively.

He joined the Department of Electronic and Computer Engineering (ECE), Hong Kong University of Science and Technology (HKUST), as a Research Associate in 2005. Then, he worked with Sony Mobile Communications, Beijing, as a Senior Antenna Engineer in 2011. He joined the ECE, HKUST again as a Research Assistant Professor in 2015. He has published 88 papers, two book chapters, and holds several patents related to antenna technology. His main research interests include the design and analysis of small antennas, MIMO antennas, applications of characteristic modes, and energy harvesting. He is also a member of IEEE Antennas and Propagation Society Education Committee (AP-S) and IEEE AP-S C. J. Reddy Travel Grant Assistant Coordinator.

BUON KIONG LAU (Senior Member, IEEE) received the B.E. degree (with Hons.) in electrical engineering from the University of Western Australia, Perth, Australia, in 1998, and the Ph.D. degree in electrical engineering from the Curtin University of Technology, Perth, in 2003.

From 2000 to 2001, he was a Research Engineer with Ericsson Research, Kista, Sweden. From 2003 to 2004, he was a Guest Research Fellow with the Department of Signal Processing, Blekinge Institute of Technology, Sweden. Since 2004, he has been with the Department of Electrical and Information Technology, Lund University, where he is currently a Professor. He has been a Visiting Researcher with the Department of Applied Mathematics, Hong Kong Polytechnic University, China; the Laboratory for Information and Decision Systems, Massachusetts Institute of Technology, Cambridge, MA, USA; and the Takada Laboratory, Tokyo Institute of Technology, Japan. His primary research interests are in various aspects of multiple antenna systems, particularly the interplay between antennas, propagation channels, and signal processing.

Prof. Lau received an award from the IEEE TRANSACTIONS ON ANTENNAS AND PROPAGATION for exceptional performance as an Associate Editor in 2015. From 2010 to 2016, he was a Track Editor, a Senior Associate Editor, and Associate Editor for the IEEE TRANSACTIONS ON ANTENNAS AND PROPAGATION. He was also a Guest Editor of the 2012 Special Issue on MIMO Technology and the Lead Guest Editor of the 2016 Special Issue on Theory and Applications of Characteristic Modes for this journal. In addition, he is a Guest Editor of the upcoming Special Issue on Artificial Intelligence in Radio Propagation for Communications for this journal. He was the Lead Guest Editor of the 2013 Special Cluster on Terminal Antenna Systems for 4G and Beyond for the IEEE ANTENNAS AND WIRELESS PROPAGATION LETTERS. From 2007 to 2010, he was a Co-Chair of Subworking Group 2.2 on "Compact Antenna Systems for Terminals" within EU COST Action 2100. From 2011 to 2015, he was a Swedish National Delegate and the Chair of Subworking Group 1.1 on "Antenna System Aspects" within COST IC1004. From 2012 to 2015, he was the Regional Delegate of European Association on Antennas and Propagation for Region 6 (Iceland, Norway, and Sweden). He was a Technical Program Committee Chair for the 2020 European Conference on Antennas and Propagation. He is a member of the Education Committee within the IEEE Antennas and Propagation Society (AP-S), where he served as the Coordinator for the annual IEEE AP-S Student Design Contest from 2013 to 2015. He was a Distinguished Lecturer for IEEE AP-S from 2017 to 2019. He is also a member of the New Technology Directions Committee for IEEE AP-S.

ROSS MURCH (Fellow, IEEE) received the bachelor's and Ph.D. degrees in electrical and electronic engineering from the University of Canterbury, New Zealand.

He is currently a Chair Professor with the Department of Electronic and Computer Engineering and a Senior Fellow with the Institute of Advanced Study with the Hong Kong University of Science and Technology, where he was the Department Head from 2009 to 2015. His unique expertise lies in his combination of knowledge from both wireless communication systems and electromagnetic areas. He has successfully supervised over 50 research graduate students. His research contributions also include more than 300 publications and 20 patents and these have attracted over 15 000 citations (Google scholar). His current research interests include Internet-of-Things, RF imaging, ambient RF systems, multiport antenna systems, and reconfigurable intelligent surfaces.

Dr. Murch has won several awards, including the Computer Simulation Technology University Publication Award. He enjoys teaching and has won two teaching awards. He has served IEEE in various positions, including an IEEE area editor, a technical program chair, a distinguished lecturer, and a fellow of evaluation committee. He is a Fellow of IET and HKIE.